Pigments of the Moss *Paraleucobryum longifolium*: Isolation and Structure Elucidation of Prenyl-Substituted 8,8′-Linked 9,10-Phenanthrenequinone Dimers

Dezső Csupor,[†,‡] Tibor Kurtán,*[,⊥] Martin Vollár,[†] Norbert Kúsz,[†] Katalin E. Kövér,[¶] Attila Mándi,[⊥] Péter Szűcs,[∥] Marianna Marschall,[∥] Seyyed A. Senobar Tahaei,[§] István Zupkó,[§] and Judit Hohmann*[,†,‡]

[†]Department of Pharmacognosy, Interdisciplinary Excellence Centre, [§]Department of Pharmacodynamics and Biopharmacy, Interdisciplinary Excellence Centre, and [‡]Interdisciplinary Centre of Natural Products, University of Szeged, Eötvös u. 6, H-6720 Szeged, Hungary

[¶]Department of Inorganic and Analytical Chemistry and [⊥]Department of Organic Chemistry, University of Debrecen, Egyetem tér 1, H-4032 Debrecen, Hungary

[∥]Department of Botany and Plant Physiology, Institute of Biology, Eszterházy Károly University, Eszterházy tér 1, H-3300 Eger, Hungary

S *Supporting Information*
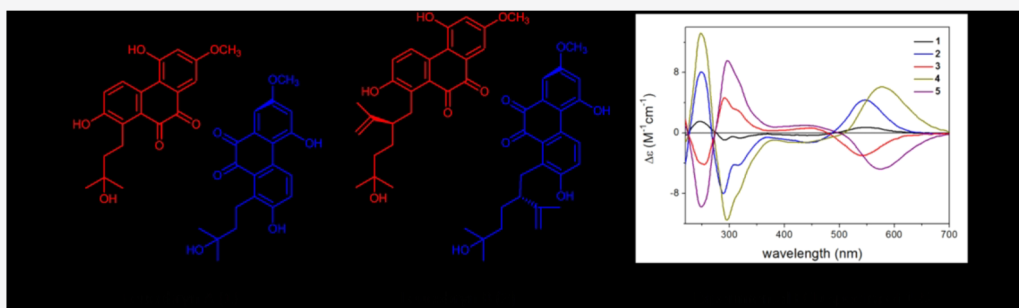
ABSTRACT: In a search for new secondary metabolites from mosses, leucobryns A−E, axially chiral 9,10-phenanthrenequinone dimers, were isolated from *Paraleucobryum longifolium* (**1**−**5**), together with diosmetin triglycoside. Leucobryns B (**2**) and C (**3**) were proved to be homodimeric atropodiastereomers containing both axial and central chirality elements, while leucobryns D (**4**) and E (**5**) were found to be heterodimeric atropodiastereomers containing central chirality in only one of the two monomeric units. Axial chirality of the compounds was determined by ECD measurements and sTDA ECD calculations, while the central chirality elements were assigned by TDDFT-SOR calculations. Leucobryns represent the first 9,10-phenanthrenequinone dimers, the monomers of which are linked through their C-8 atoms. Leucobryns B−E contain an uncommon C_{10} monoterpenoid side chain, in which isoprenoid units are joined by 3,4 linkages. Leucobryns A and B exhibited weak antiproliferative activity against several human cancer cell lines.

Bryophytes, comprising about 23 000 species worldwide, are a source of structurally unique, bioactive compounds. Although the phytochemical and pharmacological potential of bryophytes is poorly explored because of the difficulties of their collection and botanical identification, numerous new compounds have been discovered from liverworts so far, including more than 40 new carbon skeletons of terpenoids and phenolic compounds.[1−5] Many moss species have been used as medicinal plants for infections and neurological disorders and also for their nutritional value.[3−5] The biological effects ascribed to the compounds identified in liverworts are mainly related to cytotoxic, antimicrobial, antifungal, antiviral, insecticide, nematocide, enzyme inhibitory, antiallergic, muscle relaxant, and antioxidant activities.[3−6] Mono-, sesqui-, di-, and triterpenoids, highly unsaturated fatty acids, flavonoids,

bibenzyls, bis-bibenzyls, acetogenins, and phenanthrenes are the main chemical types of secondary metabolites of liverworts.[3−5]

Paraleucobryum longifolium (Ehrh. ex Hedw.) Loeske, belonging to the Dicranaceae family, is widely distributed in North America, Russia, and Europe. The plant grows on cliffs, tree trunks, stumps, and rotten logs, at moderate to high (400−2900 m) altitudes.[7] *P. longifolium* was investigated earlier for lipid constituents; wax esters, hydrocarbons, and steryl esters have been described from the plant.[8] In the present study, secondary metabolites of *P. longifolium* were analyzed with special attention to the pigments with a violet
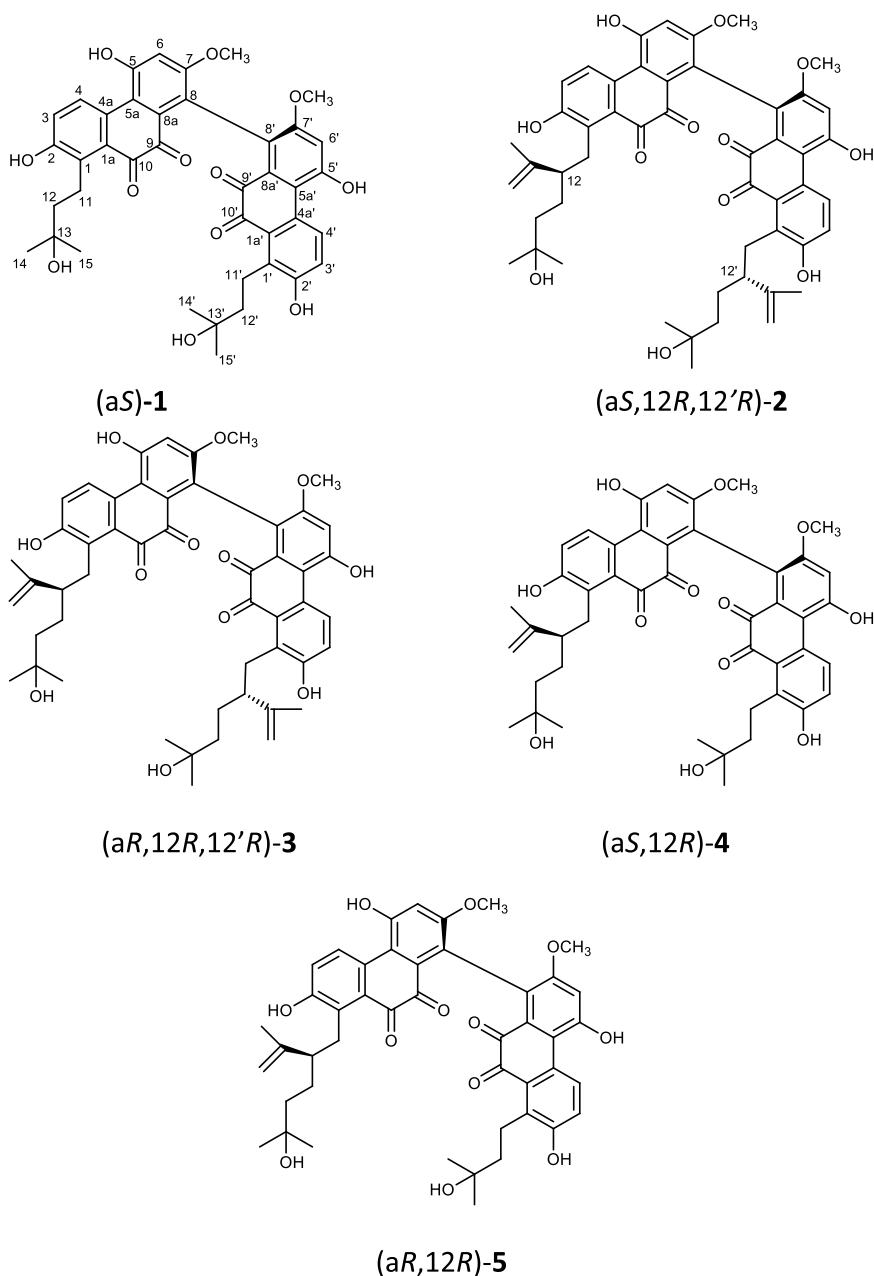
Figure 1. Structures of leucobryns A–E (1–5).

color. Herein, we report the isolation, structure determination, and pharmacological evaluation of five new 9,10-phenanthrenequinone dimers, named leucobryns A–E (1–5).

RESULTS AND DISCUSSION

P. longifolium was extracted with MeOH, and the evaporated extract was subjected to column chromatography (CC) on polyamide. Fractions eluted with 80% MeOH displayed a strong violet color. Dark violet compounds 1–5 were isolated using vacuum liquid chromatography, gel filtration on Sephadex LH-20, and RP-HPLC.

Compound 1 was obtained as a dark violet amorphous powder with UV maxima at 542.5, 370, 305, 272, and 213.5 nm. The molecular formula was established as $C_{40}H_{38}O_{12}$ based on HRESIMS data, which showed the sodium adduct ion $[M + Na]^+$ at m/z 733.2252 (calcd for 733.2255 $C_{40}H_{38}O_{12}Na$). The ^{13}C JMOD spectrum displayed 20

resonances, which indicated that compound 1 is a symmetric dimer (Figure 1).

The monomeric moiety of the molecule is constructed by 10 nonprotonated carbons (δ_C 71.98, 118.00, 121.19, 129.50, 131.07, 131.23, 133.91, 155.84, 156.81, and 157.65), two carbonyl (δ_C 192.01 and 192.77), three methines (δ_C 107.65, 122.06, and 129.97), two methylenes (δ_C 23.07 and 44.21), a methoxy group (δ_C 56.29), and two methyls (δ_C 28.86 and 28.99) (Table 1). The evaluation of 1D ^1H and 2D $^1H-^1H$ COSY spectroscopic data revealed the presence of two *ortho*-doublets (δ_H 8.44 d, 7.04 d), an isolated aromatic proton (δ_H 6.79 s), an ethylene group (δ_H, 3.00 td, 2.87 td, 1.74 td, 1.65 td), two methyls [δ_H 1.28 s (6H)], and a methoxy group [δ_H 3.65 s (3H)] (Table 2). HMBC correlations between H-6 and C-5, C-7, C-8, and C-5a, between H-3 and C-1, C-2, C-4, and C-4a, and between H-4 and C-2, C-1a, and C-10 disclosed that compound 1 contains a 9,10-phenanthrenedione parent system

Table 1. ¹³C NMR Data of Compounds 1−5 (Methanol-d_4, T = 298 K, δ ppm)

position	1[a]	2[b]	3[b]	4[b]	5[b]
1	133.91	132.32	132.30	132.29	132.30
1a	129.50	130.39	130.20	130.21	130.37
2	155.84	156.31	156.35	156.35	156.31
3	122.06	121.70	121.81	121.81	121.69
4	129.97	129.95	129.98	129.97	129.95
4a	131.07	130.94	131.10	131.09	130.95
5	156.81	156.73	156.74	156.75	156.71[f]
5a	118.00	118.15	118.12	118.13	118.13
6	107.65	107.62	107.60	107.65	107.67[g]
7	157.65	157.44	157.78	157.61	157.47[e]
8	121.19	120.83	120.96	120.97	120.95[c]
8a	131.23	131.14	130.94	130.95[c]	130.91[h]
9	192.01	n. o.	192.38	192.44[d]	192.68[d]
10	192.77	192.06	193.57	193.68	193.81
11	23.07	31.26	31.84	31.22	31.25
12	44.21	50.13	50.02	50.04	50.12
13	71.98	148.85	149.07	149.07	148.83
14	28.99	112.61	112.29	112.30	112.60
15	28.86	18.56	18.59	18.58	18.54
16		28.28	28.04	28.05	28.13
17		42.85	42.84	42.83	42.85
18		71.46	71.47	71.46	71.46
19		29.30	29.30	29.28	29.30
20		28.88	28.86	29.00	28.99
1′	133.91	132.32	132.30	133.92	133.92
1′a	129.50	130.39	130.20	129.51	129.52
2′	155.84	156.31	156.35	155.84	155.84
3′	122.06	121.70	121.81	122.06	122.05
4′	129.97	129.95	129.98	129.97	129.95
4a′	131.07	130.94	131.10	131.25	131.25
5′	156.81	156.73	156.74	156.88	156.79[f]
5a′	118.00	118.15	118.12	118.01	118.01
6′	107.65	107.62	107.60	107.65	107.60[g]
7′	157.65	157.44	157.78	157.85	157.60[e]
8′	121.19	120.83	120.96	121.17	121.06[c]
8a′	131.23	131.14	130.94	131.09[c]	131.25[h]
9′	192.01	n. o.	192.38	191.98[d]	191.96[d]
10′	192.77	192.06	193.57	192.67	192.68
11′	23.07	31.26	31.24	23.06	23.07
12′	44.21	50.13	50.02	44.21	44.22
13′	71.98	148.85	149.07	71.98	71.98
14′	28.99	112.61	112.29	28.86	28.88
15′	28.86	18.56	18.59	28.86	28.88
16′		28.28	28.04		
17′		42.85	42.84		
18′		71.46	71.47		
19′		29.30	29.30		
20′		28.88	28.86		
7-OCH₃,	56.29	56.27	56.28	56.28	56.28
7′-OCH₃	56.29	56.27	56.28	56.28	56.28

[a]125 MHz. [b]175 MHz; n.o. not observed. [c,d,e,f,g,h]Signals in each column are interchangeable.

with O-functionalities at C-2 (δ_C 155.84), C-5 (δ_C 156.81), and C-7 (δ_C 157.65) and C-functionalities at C-1 (δ_C 133.91) and C-8 (δ_C 121.19) (Figure 2). The alternative anthraquinone structure was ruled out because the strong HMBC cross-peak observed between H-4 and C-5a suggested that they are separated by three rather than four bonds. The other three-

bond correlations of H-4 with C-2 and C-1a had similar intensities. On the other hand, a weak four-bond heteronuclear interaction was detected between H-4 and the carbonyl carbon at $\delta_{C\text{-}10}$ 192.77. Furthermore, the proposed structure was confirmed by a weak cross-peak exhibited between H-6 and C-4a, which would not be expected in an anthraquinone, due to the long distance (5 bonds) between these atoms.

The presence of the methoxy group at C-7 was established by HMBC correlations between the OCH₃ protons and C-7 and C-6 and by a NOESY cross-peak between H-6 and the OCH₃ group. A 3-hydroxyisopentyl substituent was corroborated with the HMBC cross-peaks observed between the methyl protons at δ_H 1.28 (H₃-14, H₃-15) and C-13 (δ_C 71.98) and C-12 (δ_C 44.21); this group was placed at C-1 on the basis of the H-11/C-1, H-11/C-1a, H-11/C-2, and H-12/C-1 HMBC correlations. A hydroxy group, concluded from the HRESIMS data, is attached at C-7, as confirmed by its chemical shift value of δ_C 157.65. In accordance with all these data, the structure of compound **1**, named leucobryn A, could be established as a dimer in which the monomers are connected via their C-8 atoms as depicted in Figure 1.

Compound **2** possessed a molecular formula of $C_{50}H_{54}O_{12}$ as determined by the HRESIMS ion at m/z 869.3505 [M + Na]⁺ (calcd for 869.3507, $C_{50}H_{54}O_{12}Na$). The ¹H NMR and ¹³C JMOD spectra revealed a structure containing 25 carbon atoms only, suggesting a symmetric dimeric structure, similarly to compound **1**. The ¹H NMR and ¹³C JMOD spectra of **2** also resembled those of **1**. In particular, the ¹H and ¹³C chemical shifts of the 9,10-phenanthrenedione part were close to those of **1** (Tables 1 and 2). The main differences were found in the C_5 prenyl side chain, which was changed to a C_{10} moiety in **2**. Combined analysis of ¹H NMR, ¹³C JMOD, and HSQC spectra proved that this C_{10} substituent consists of a nonprotonated, oxygenated carbon (δ_C 71.46), a disubstituted carbon−carbon double bond (δ_H 4.41 d, 4.57 dq; δ_C 112.61, 148.85), three sp^3 methylenes [δ_H 1.25 m, 1.36 m, 1.48 m (2H), 2.97 dd, 3.15 dd; δ_C 28.28, 31.26, 42.85], a methine (δ_H 2.31 m; δ_C 50.13), and three methyl groups (δ_H 1.11 s, 1.12 s, 1.64 br s; δ_C 18.56, 28.88, 29.30). Based on the ¹H−¹H COSY spectrum, two structural fragments could be unambiguously assigned for the C_{10} part: −CH₂−CHR−CH₂−CH₂− (A) and CH₂=(CH₃)C− (B) (Figure 3).

Structural fragment A (C-11−C-12−C-16−C-17) was connected to the phenanthrenedione skeleton based on the long-range C−H correlations of H-11/C-1a, H-11/C-1, and H-11/C-2. In addition, a 2-hydroxyisopropyl group, attached to C-17, was confirmed by the HMBC correlations between H₃-19/C-17, H₃-19/C-18, and H₃-20/C-17. HMBC cross-peaks between H-14/C-12, H-15/C-12, and H-12/C-13 unambiguously established that unit B (C-13−C-14−C-15) is linked to C-12. The data above provided evidence for a C_{10} monoterpene side chain, in which, interestingly, the isoprenoid units are joined by 3,4 linkages, instead of the regular head-to-tail, tail-to-tail, or head-to-head connection. Collectively, the structure of compound **2** was established as shown in Figure 1 and named leucobryn B.

Compound **3** (leucobryn C) was isolated the same way as **2**, and in the final step of the purification procedure compounds **2** and **3** were separated by RP-HPLC. The HRESIMS data of **3** displayed a sodium adduct ion at m/z 869.3507 [M + Na]⁺, indicating the same molecular formula of $C_{50}H_{54}O_{12}$ as that of compound **2**. 1D and 2D ¹H/¹³C NMR characteristics of **2** and **3** were similar, with only minute differences observed in the

Table 2. ^{1}H NMR Data of Compounds 1−5 in Methanol-d_4 at T = 298 K (δ ppm, J Hz)

position	1[a]	2[b]	3[b]	4[b]	5[b]
3	7.04, d (8.9)	7.00, d (8.9)	7.01, d (8.9)	7.01, d (8.9)	7.01, d (8.9)
4	8.44, d (8.9)	8.40, d (8.9)	8.38, d (8.9)	8.39, d (8.9)	8.39, d (8.9)
6	6.79, s	6.78, s	6.79, s	6.79, s	6.79, s
11a	3.00, td (11.6, 4.9)	3.15, dd (12.7, 8.0)	3.14, dd (12.6, 7.2)	3.13, dd (12.6, 7.2)	3.15, dd (12.5, 8.1)
11b	2.87, td (11.6, 4.9)	2.97, dd (12.7, 6.5)	2.97, dd (12.6, 7.2)	3.02, m	2.97, dd (12.5, 6.5)
12a	1.74, td (12.7, 5.0)	2.31, m	2.30, m	2.30, m	2.31, m
12b	1.65, td (12.7, 5.0)				
14a	1.28, s	4.57, dq (2.3, 1.4)	4.54, dq (2.3, 1.4)	4.59, br s	4.57, br s
14b		4.41, d (2.3)	4.47, d (2.3)	4.46, br s	4.40, br s
15	1.28, s	1.64, br s	1.67, br s	1.67, s	1.64, s
16		1.48, m (2H)	1.41, m (2H)	1.41, m (2H)	1.47, m (2H)
17		1.36, m	1.35, m	1.34, m	1.36, m
		1.25, m	1.21, m	1.21, dd (13.0, 4.3)	1.25, m
19		1.12, s	1.11, s	1.10, s	1.12, s
20		1.11, s	1.09, s	1.09, s	1.11, s
3′	7.04, d (8.9)	7.00, d (8.9)	7.01, d (8.9)	7.04, d (8.9)	7.05, d (9.0)
4′	8.44, d (8.9)	8.40, d (8.9)	8.38, d (8.9)	8.45, d (8.9)	8.45, d (8.8)
6′	6.79, s	6.78, s	6.79, s	6.80, s	6.79, s
11′a	3.00, td (11.6, 4.9)	3.15, dd (12.7, 8.0)	3.15, dd (12.6, 7.2)	3.00, m	3.00, td (11.9, 4.7)
11′b	2.87, td (11.6, 4.9)	2.97, dd (12.7, 6.5)	2.97, dd (12.6, 7.2)	2.89, td (11.8, 4.7)	2.89, td (11.6, 4.7)
12′a	1.74, td (12.7, 5.0)	2.31, m	2.30, m	1.73, td (13.0, 4.7)	1.74, td (13.0, 4.7)
12′b	1.65, td (12.7, 5.0)			1.66, m	1.68, td (12.3, 4.6)
14′a	1.28, s	4.57, dq (2.3, 1.4)	4.54, dq (2.3, 1.4)	1.27, s	1.28, s
14′b		4.41, d (2.3)	4.47, d (2.3)		
15′	1.28, s	1.64, br s	1.67, br s	1.27, s	1.28, s
16′		1.48, m (2H)	1.41, m (2H)		
17′		1.36, m	1.35, m		
18′		1.25, m	1.21, m		
19′		1.12, s	1.11, s		
20′		1.11, s	1.09, s		
7-OCH$_3$	3.65, s	3.65, s	3.67, s	3.66, s	3.65, s
7′-OCH$_3$	3.65, s	3.65, s	3.67, s	3.66, s	3.65, s

[a]500 MHz. [b]700 MHz.
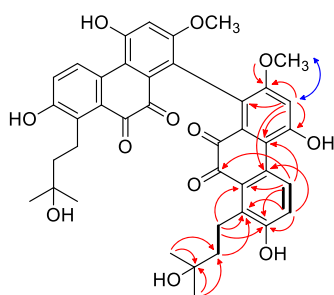
Figure 2. Key 2D NMR correlations in compound 1; —— bold line: ^{1}H−^{1}H COSY, → red arrows: HMBC, ↔ blue arrow: NOESY.

Figure 3. Key 2D NMR correlations in the monoterpenoid part of 2; —— bold line: ^{1}H−^{1}H COSY, → red arrows: HMBC.

chemical shifts of H-14, H-16, C-10, C-11, and C-14 (Tables 1 and 2). These data suggest that the structural differences are explicable in terms of the stereochemistry of the compounds.

Compound 4 (leucobryn D) was isolated as a dark violet amorphous solid. HRESIMS data revealed a molecular formula of $C_{45}H_{46}O_{12}$ according to the sodium adduct ion at m/z 801.2876 $[M + Na]^+$ (calcd for $C_{45}H_{46}O_{12}Na$ 801.2881). ^{1}H NMR and ^{13}C JMOD data contained signals similar to the resonances of both compounds 1 and 2 (Tables 1 and 2), indicating that compound 4 is a heterodimer constructed by the monomeric moieties of 1 and 2. As in compounds 1 and 2, the monomeric constituents of 4 are connected via their C-8 atoms. 2D NMR studies provided further evidence to confirm
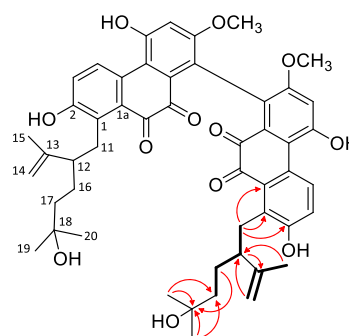
the structure of this compound as depicted in structural formula 4.

Compound 5 (leucobryn E) was separated from 4 by RP-HPLC using a gradient system of MeCN−H$_2$O mixtures. All HRESIMS and NMR characteristics of compound 5 were highly similar to those of 4, suggesting a molecular pair with the same 2D structure, but with different chirality.

In addition, diosmetin 7-O-[2,4-di-O-(α-L-rhamnopyrano-syl)]-β-D-glucopyranoside was also isolated from *P. longifolium* and identified based on NMR data (Table S1, Supporting Information).

For the configurational assignment of the axial chirality elements of **1**−**5**, conformational analysis and the sTDA (simplified Tamm−Dancoff approximation) approach[9] were applied on the arbitrarily chosen (aS,12R,12′R)-**2** and (aR,12R,12′R)-**3** stereoisomers differing in the axial chirality. When both central and axial chirality elements are present in biaryl compounds, the ECD spectrum is governed by the axial chirality element, which can be elucidated by ECD calculations.[10] The experimental ECD spectrum of **1**, containing only an axial chirality element, was found to be similar to those of **2** and **4**, but with weaker intensity, and nearly mirror-images of the ECD spectra of **3** and **5** were recorded, indicating that the central chirality elements of **2**−**5** do not significantly contribute to the ECD spectra (Figure 4a).
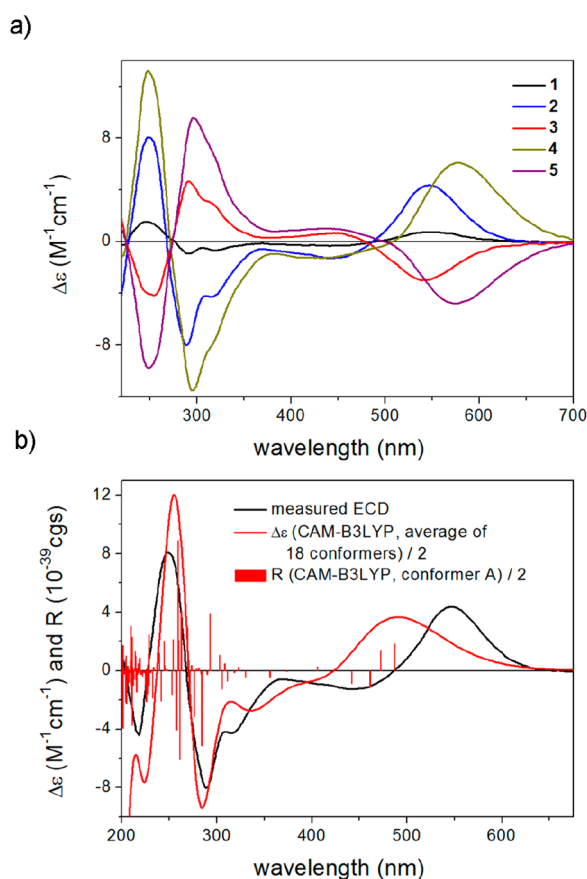
mol, which is considered the minimum rotational energy barrier for the presence of separable atropisomers.[15]

Biaryls **1**−**5** are expected to have a large number of ECD transitions to compute, which required the use of the sTDA method[9c,d] developed for large molecules and/or for compounds with a large number of ECD transitions. This method was developed for complex molecules, the TDDFT calculation of which would be quite demanding computationally or not feasible at an advanced DFT level. Despite the strengths of this method, there are only a few examples for application in the field of natural products.[16,17] The initial Merck Molecular Force Field (MMFF) conformational search of (12R,12′R)-**2**/**3** resulted in 1326 conformers in a 21 kJ/mol energy window, including both the (aS,12R,12′R)-**2** and (aR,12R,12′R)-**3** stereoisomers, which were separated manually. Subsequently, they were reoptimized at the AM1 semiempirical level to reduce the number of conformers[18] and then at the CAM-B3LYP/TZVP[19] PCM/MeCN level.

sTDA-ECD calculations were performed for conformers above 1% population at the CAM-B3LYP, LC-BLYP,[20] and ωB97X[21] levels, for which the required single-point calculations were performed with the same functionals and the TZVP basis set. All of the Boltzmann-averaged ECD spectra of (aS,12R,12′R)-**2** and (aR,12R,12′R)-**3** consistently gave moderate to good agreement with the experimental ECD spectrum of **2** and **3**, respectively, and all the low-energy conformers of the same axial chirality exhibited similar ECD spectra, permitting the elucidation of the absolute configuration of the axial chirality as (aS) in **2** and (aR) in **3** (Figure 4b and Figure 5).
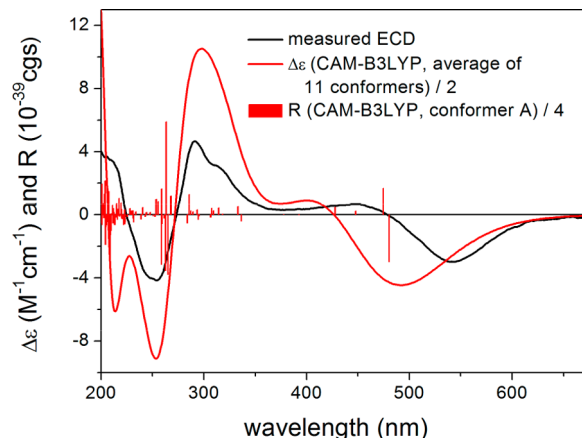

Figure 4. (a) Comparison of the experimental ECD spectra of **1**−**5** measured in MeCN; (b) comparison of the experimental ECD spectrum of **2** in MeCN to the sTDA-CAM-B3LYP spectrum of (aS,12R,12′R)-**2** computed from the CAM-B3LYP/TZVP single-point data. Level of optimization: CAM-B3LYP/TZVP PCM/MeCN. Bars represent the rotational strength values of the lowest-energy conformer.

Figure 5. Comparison of the experimental ECD spectrum of **3** in MeCN with the sTDA-CAM-B3LYP ECD spectrum of (aR,12R,12′R)-**3** computed from the CAM-B3LYP/TZVP single-point data. Level of optimization: CAM-B3LYP/TZVP PCM/MeCN. Bars represent the rotational strength values of the lowest-energy conformer.

In axially chiral biaryls, the absolute configuration of the central chirality elements was determined by ECD analysis of the monomers co-isolated from the same source[11,12] or, alternatively, by VCD calculations.[13] The configurational assignment of both central and axial chirality elements in axially chiral natural biaryls is considered a challenging task by even the combination of different chiroptical methods and their computation.[10a,11a,14] Owing to the substitution pattern in the *ortho*-positions of the biaryl axis, biaryls **1**−**5** were expected to have a rotational energy barrier exceeding 93.6 kJ/

Thus, compounds **2** and **3** are atropodiastereomers with identical absolute configuration of their stereogenic centers. Comparing the ECD spectra of **1**, **4**, and **5** to those of **2** and **3** revealed the absolute configuration of **1** and **4** as (aS) and that of **5** as (aR) (Figure 4a).

Since both the experimental and computed ECD spectra of (aS,12R,12′R)-**2** and (aR,12R,12′R)-**3** showed a mirror-image relationship, in principle the determination of the central chirality element was not feasible with the ECD spectra.

However, the experimental specific rotation (SR) values of **2** and **3** had different magnitudes with opposite signs [**2**: $[\alpha]^{23}_D$ = +162, **3**: $[\alpha]^{23}_D$ = −222], which suggested that the SR values are also influenced by the central chirality elements, although the different signs derived from the different axial chirality. In order to elucidate the absolute configuration of the central chirality elements, SR calculations of (aS,12R,12′R)-**2** and (aR,12R,12′R)-**3** were performed on the CAM-B3LYP/TZVP PCM/acetone conformers.[22] Considering that **2** and **3** are homodimers with identical C-12 and C-12′ absolute configuration in the monomeric units, the (aS,12R,12′R)-**2** and (aR,12R,12′R)-**3** stereoisomers fully cover all four possibilities. In line with the ECD results, Boltzmann-averaged SR values computed at four levels of theory for (aS,12R,12′R)-**2** showed consistently positive values ranging from 46.5 to 161.6 vs the experimental SR value of 162, while those computed for (aR,12R,12′R)-**3** gave negative values with larger magnitude in the range of −102.8 to −234.0 vs the experimental SR of −222. Although the magnitude of computed SRs can be considerably different from that of the experimental ones,[23] all four applied combinations of levels showed a clear tendency with larger absolute values for the (aR,12R,12′R) configuration compared to those of (aS,12R,12′R). A good agreement for the B3LYP/TZVP PCM/acetone // CAM-B3LYP/TZVP PCM/acetone level [161.6 vs experimental 162 for (aS,12R,12′R)-**2** and −234.0 vs experimental −222 for (aR,12R,12′R)-**3**)] permitted a probable assignment of the central chirality as (aS,12R,12′R)-**2** and (aR,12R,12′R)-**3**. The wavelength of experimental SR values measured at the sodium D line (589.3 nm) falls in the higher-wavelength range of the highest-wavelength ECD transition of **2** and **3**, and they had the same signs as those of the corresponding ECD transition.[24] In order to check that the SR values of **2** and **3** recorded at 589.3 nm belong to the monotonously increasing wavelength range of the ORD spectrum without a change of sign (ORD anomaly) or they contain the effect of the ORD anomaly, SR values of (aS,12R,12′R)-**2** and (aR,12R,12′R)-**3** were calculated at 10 selected wavelengths in the range of 575−800 nm with four methods (Figures 6 and 7). These SR calculations consistently
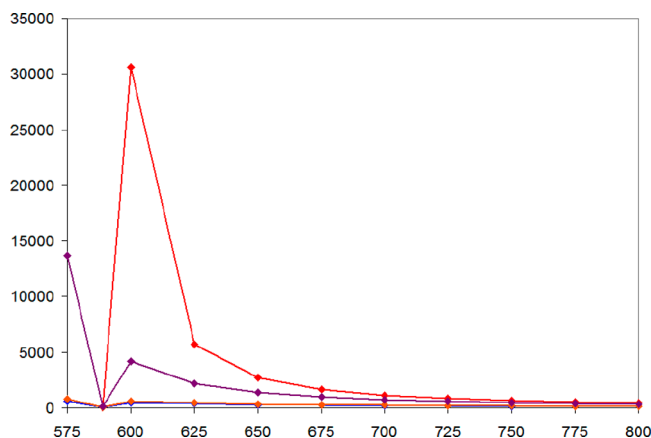
Figure 7. Average SR values of (aR,12R,12′R)-**3** computed at various wavelengths at four levels of theory (red: B3LYP/TZVP PCM/acetone, blue: BH&HLYP/TZVP PCM/acetone, orange: CAM-B3LYP/TZVP PCM/acetone, purple: PBE0/TZVP PCM/acetone) with the TZVP basis set and PCM solvent model for acetone. Level of optimization: CAM-B3LYP/TZVP PCM/acetone.
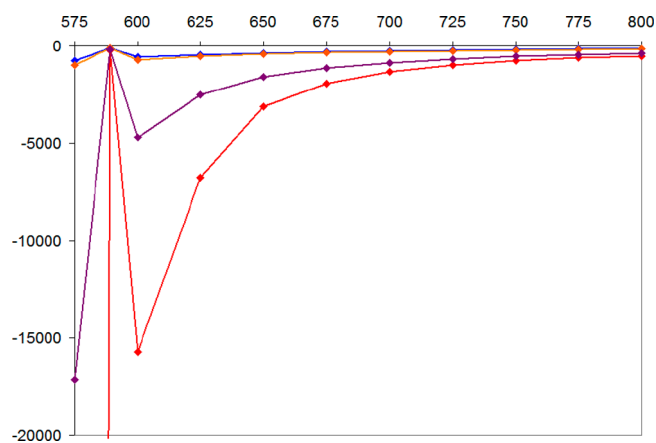
showed that there was no sign inversion of SR values in the 600−800 nm wavelength range, while anomalous ORD appears around the wavelength of the sodium D line. The ORD anomaly expected below 600 nm and the MMFF-AM1-clustering-DFT reoptimization sequence for the conformational analysis to reproduce the biaryl dihedral angles and the side-chain conformation may expose some uncertainty in the determination of the central chirality. However, the computed SR values clearly support the conclusion, and characteristic differences in the magnitudes of the computed SR values for (aS,12R,12′R)-**2** and (aR,12R,12′R)-**3** appeared consistently at all the computed wavelengths.[25]

The SR calculations of (aS,12R,12′R)-**2** and (aR,12R,12′R)-**3** represent the first example to determine the central chirality of a homodimeric biaryl natural product in the presence of axial chirality on the basis of the SR calculations. VCD measurement and calculations were reported earlier to determine both axial and central chirality for the biaryl natural product (aS,2R,2′R)-cephalochromin, the SR calculation of which could not decide on the central chirality.[13] However, the same VCD approach failed to determine the central chirality of flavomannin A in the presence of axial chirality.[10a] SR calculations were also successfully utilized to determine the central chirality of quinolinophane derivatives containing both planar and central chirality elements.[26] The recent example of leucobryns B and C also demonstrated that the specific rotation values can contain stereochemical information, which are either missing from or supplementary to the ECD data, and it can be utilized to determine stereochemical properties, which would not be feasible by using only ECD calculations.

Phenanthrenes are characteristic compounds of bryophytes. The first derivative, 2-hydroxy-3,7-dimethoxyphenanthrene, was isolated from *Marchantia polymorpha* by Asakawa et al.[27] To date, about two dozen compounds belonging to phenanthrenes, 9,10-dihydrophenanthrenes, biphenanthrenes, and bisbibenzyl-phenanthrenes were isolated from different genera of bryophytes.[1,28−36] Leucobryns (**1**−**5**) are the first representatives of dimeric phenanthrenes with a 9,10-*ortho*-quinone structure. Monomeric 9,10-phenanthraquinones are extremely rare in nature: previously such compounds have only been isolated from some lichens,[37] bacteria,[38−40] and vascular

Figure 6. Average SR values of (aS,12R,12′R)-**2** computed at various wavelengths at four levels of theory (red: B3LYP/TZVP PCM/acetone, blue: BH&HLYP/TZVP PCM/acetone, orange: CAM-B3LYP/TZVP PCM/acetone, purple: PBE0/TZVP PCM/acetone) with the TZVP basis set and PCM solvent model for acetone. Level of optimization: CAM-B3LYP/TZVP PCM/acetone.

plant species.[41,42] 9,10-Phenanthraquinones produced by microorganism have been reported to have strong antibiotic properties and antiviral activity.[35,36]

The possible biogenetic origin of phenanthraquinones is rarely discussed in the literature. Regarding their oxygenation patterns, acetate-derived polyketide biogenesis was suggested for some phenanthraquinones based on isotope feeding experiments.[36,43,44] On the other hand, phenanthrenes can be formed by intramolecular oxidative *ortho*-coupling of dihydrostilbenes (bibenzyls).[45] In such cases the hydroxylation/methoxylation pattern of at least one of the two aromatic rings in phenanthrene corresponds to the 3,5-disubstitution pattern of stilbenes. This structural feature is also characteristic of leucobryns. Considering that bibenzyls and bis-bibenzyls belong to the most important secondary metabolites of bryophytes, their biogenetic relationship with dimeric phenanthraquinones can be accepted. The occurrence of bibenzyl–phenanthrene and bibenzyl–dihydrophenanthrene compounds in some bryophytes (*Buzzania* and *Cavicularia* species)[24,25] provides further evidence for the presumption that leucobryns are biosynthesized by dimerization of bibenzyls with a C–C linkage, followed by oxidative steps yielding a 9,10-dioxo functionality. Similar to leucobryns **1**−**5**, certain bibenzyls are also substituted with prenyl or geranyl groups.[1,2]

The antiproliferative action of the isolated compounds (**1**−**5**) was determined against four human cancer cell lines of gynecological origin, but only moderate (<10 μM) or negligible activities were measured (Table S6).

■ EXPERIMENTAL SECTION

General Experimental Procedures. UV spectra were measured on a Shimadzu UV-1800 UV−vis spectrophotometer in MeOH. The NMR spectra were recorded in methanol-d_4 on a Bruker Avance DRX 500 spectrometer operating at 499.9 MHz for ^{1}H and 125.7 MHz for ^{13}C and a Bruker Avance NEO 700 spectrometer operating at 700.25 MHz (^{1}H) and 176.08 MHz (^{13}C), respectively. All measurements were performed at 298 K. The signals of the methanol-d_4 ([1]H: 3.35 ppm, [13]C: 49.3 ppm) were taken as reference. 2D NMR data were acquired and processed with Bruker TopSpin 4.0.5 software. Standard pulse programs available in the Bruker library were used for 2D [1]H−^{1}H magnitude COSY (*cosygpqf*), gradient- and sensitivity-enhanced HSQC (*hsqcetgpsisp2.2*), magnitude HMBC (*hmbcgplpndqf*), and EASY-ROESY (*roesyadjsph*) experiments. The high-resolution MS spectra were acquired on an FTHRMS-Orbitrap (Thermo-Finnigan) mass spectrometer equipped with an ESI ion source in positive ionization mode. HPLC was performed on a Waters 600 HPLC system (Waters Corporation, Milford, USA), equipped with a 2998 photodiode array detector and online degasser. ECD spectra were recorded on a JASCO J-810 spectropolarimeter. Solvents were distilled prior to use, and spectroscopic grade solvents were applied for spectroscopic measurements.

Plant Material. *Paraleucobryum longifolium* (Dicranaceae) was collected in Mátrafüred (Hungary) in June 2016. A voucher specimen (No. 883) has been deposited in the Herbarium of the Department of Pharmacognosy of University of Szeged, Szeged, Hungary. The plant material was dried at room temperature and chopped in a Retsch SM 100 chopper.

Extraction and Isolation. The plant material (4.0 kg) was extracted in a percolator with 75 L of MeOH at room temperature. The extract was evaporated (331.1 g) and the residue was subjected to column chromatography on polyamide using MeOH−H$_2$O mixtures (20%, 40%, 60%, 80%, 100%). Fractions obtained with 80% MeOH contained compounds with a violet-black color. The 80% MeOH fraction was further separated by vacuum liquid chromatography (VLC) on normal-phase silica gel (particle size 45−63 μm) with a gradient system of CHCl$_3$−MeOH (10:0, 9.6:0.4, 9.3:0.7, 9:1,

8:2, 7:3, and 0:1). This separation yielded 12 subfractions; among them subfractions 9−12 contained a MeOH-soluble, but a CHCl$_3$-insoluble violet-black material, and subfraction 9 was chosen for further purification on NP-CC (silica gel, particle size 45−63 μm) using toluene−CHCl$_3$−MeOH (4:12:3) as eluent. This chromatography afforded subfractions A−I; the violet-black material was concentrated in subfractions D, E, and F. Subfraction D was separated by reversed-phase flash chromatography (FC) using a gradient system of MeCN−H$_2$O mixtures (from 50% to 50% to 100% MeCN)], then by gel filtration on Sephadex LH-20 eluted with MeOH, and finally by RP-HPLC on a Kinetex XB-18 column (100 A, 250 × 4.6 mm, 5 μm, Phenomenex, Torrance, CA, USA) using a H$_2$O−MeCN gradient system (0 min: H$_2$O−acetonitrile 6:4, 1 min: 6:4, 10 min: 4:6, 11 min: 1:9, 12 min: 6:4, 17 min: 6:4) as eluent at a flow rate of 1.5 mL/min. By this means leucobryn B (**2**) (0.8 mg, t_R = 9.95 min) and leucobryn C (**3**) (0.65 mg, t_R = 10.27 min) were separated. Subfraction E was chromatographed on Sephadex LH-20 eluted with MeOH and further purified by RP-HPLC on a Kinetex XB-18 column. The detection was in the full UV wavelength range. Elution was carried out with the gradient system of H$_2$O−MeCN (0 min: H$_2$O−MeCN 65:35, 1 min: 65:35, 10 min: 62:38, 12 min: 62:38, 13 min: 0:100, 13.5 min: 65:35, 18 min: 65:35) at a flow rate of 1.5 mL/min, affording leucobryn E (**5**) (0.6 mg, t_R = 14.42 min) and leucobryn D (**4**) (0.6 mg, t_R = 14.96 min). Subfraction F was chromatographed on Sephadex LH-20 with MeOH, yielding the pure compound leucobryn A (**1**) (3.6 mg). The 60% MeOH fraction of the polyamide column was subjected to VLC on normal-phase silica gel (particle size 45−63 μm) using a gradient system of cyclohexane−CHCl$_3$−MeOH (90:9.9:0.1, 80:19.8:0.2, 70:29.7:0.3, 0:9:1, 0:8:2, 0:7:3, 0:6:4, 0:5:5, 0:4:6, 0:3:7, 0:2:8, and 0:0:1). The separation yielded subfractions A−R, and subfraction M was selected for further purification on RP-VLC with a gradient system of H$_2$O−MeOH (6:4, 5:5, 4:6, 3:7, 2:8, and 0:1) and yielded subfractions 1−9. Subfraction 1 was purified by gel filtration on Sephadex LH-20 with MeOH and by RP-HPLC on Kinetex C-18 (100 A, 150 × 4.6 mm, 5 μm, Phenomenex) using a H$_2$O−isopropanol (IPA) gradient system (0 min: H$_2$O−IPA 9:1, 1 min: 9:1, 10 min: 4:6, 11 min: 3:7, 12 min: 9:1, 18 min: 9:1) as eluent at a flow rate of 1 mL/min. This separation afforded diosmetin 7-O-[2,4-di-O-(α-L-rhamnopyranosyl)]-β-D-glucopyranoside (t_R = 9.93 min). This compound was described previously from the bryophyte *Dicranum scoparium* Hedw.[46]

Leucobryn A (1): purple, amorphous solid; $[\alpha]^{23}_D$ +316 (*c* 0.03, acetone); UV λ_{max} (log ε) 542.5 (3.40), 370 (3.55), 305 (4.14), 272 (4.50), 213.5 (4.64) nm; ECD (MeCN, λ [nm] ($\Delta\varepsilon$), c 0.087 mM) 550 (+0.75), 441 (−0.33), 318sh (−0.67), 291 (−0.92), 248 (+1.53), 221sh (−0.25); ^{1}H NMR (700 MHz, methanol-d_4) see Table 1; ^{13}C NMR (175 MHz, methanol-d_4) see Table 2; HRESIMS (positive) *m/z* 733.2252 [M + Na]$^+$, calcd for 733.2255 C$_{40}$H$_{38}$O$_{12}$Na, *m/z* 749.2002 [M + K]$^+$, calcd for 749.1995 C$_{40}$H$_{38}$O$_{12}$K.

Leucobryn B (2): purple, amorphous solid; $[\alpha]^{23}_D$ +162 (*c* 0.07, acetone); ECD (MeCN, λ [nm] ($\Delta\varepsilon$), c 0.066 mM) 547 (+4.36), 441 (−1.26), 316sh (−4.27), 289 (−8.01), 249 (+8.09), 218 (−4.43); ^{1}H NMR (700 MHz, methanol-d_4) see Table 1; ^{13}C NMR (175 MHz, methanol-d_4) see Table 2; HRESIMS (positive) *m/z* 869.3505 [M + Na]$^+$, calcd for 869.3507 C$_{50}$H$_{54}$O$_{12}$Na, *m/z* 885.3249 [M + K]$^+$, calcd for 885.3247 C$_{50}$H$_{54}$O$_{12}$K.

Leucobryn C (3): purple, amorphous solid; $[\alpha]^{23}_D$ −222 (*c* 0.08, acetone); ECD (MeCN, λ [nm] ($\Delta\varepsilon$), c 0.044 mM) 540 (−2.99), 446 (+0.67), 313sh (+3.09), 291 (+4.66), 254 (−4.17), 247sh (−3.98), 216sh (+2.85); ^{1}H NMR (700 MHz, methanol-d_4) see Table 1; ^{13}C NMR (175 MHz, methanol-d_4) see Table 2; HRESIMS (positive) *m/z* 869.3507 [M + Na]$^+$, calcd for 869.3507 C$_{50}$H$_{54}$O$_{12}$Na, *m/z* 885.3258 [M + K]$^+$, calcd for 885.3247 C$_{50}$H$_{54}$O$_{12}$K.

Leucobryn D (4): purple, amorphous solid; $[\alpha]^{23}_D$ +160 (*c* 0.07, acetone); ECD (MeCN, λ [nm] ($\Delta\varepsilon$), c 0.064 mM) 577 (+6.09), 431 (−1.26), 314sh (−8.19), 295 (−11.52), 255sh (12.08), 248 (+13.19), 221sh (−1.11); ^{1}H NMR (700 MHz, methanol-d_4) see Table 1; ^{13}C NMR (175 MHz, methanol-d_4) see Table 2; HRESIMS (positive) *m/*

z 801.2874 $[M + Na]^+$, calcd for 801.2881 $C_{45}H_{46}O_{12}Na$, m/z 817.2624 $[M + K]^+$, calcd for 817.2621 $C_{45}H_{46}O_{12}K$.

Leucobryn E (5): purple, amorphous solid; $[\alpha]^{23}_D$ −357 (c 0.03, acetone); ECD (MeCN, λ [nm] ($\Delta\varepsilon$), c 0.065 mM) 575 (−4.77), 436 (+1.03), 317sh (+6.83), 297 (+9.56), 258sh (−8.63), 248 (−9.77), 220sh (+0.94); ^1H NMR (700 MHz, methanol-d_4) see Table 1; ^{13}C NMR (175 MHz, methanol-d_4) see Table 2; HRESIMS (positive) m/z 801.2876 $[M + Na]^+$, calcd for 801.2881 $C_{45}H_{46}O_{12}Na$, m/z 817.2617 $[M + K]^+$, calcd for 817.2621 $C_{45}H_{46}O_{12}K$.

Computational Section. Mixed torsional/low-frequency mode conformational searches were carried out by means of the MacroModel 10.8.011 software by using the MMFF with an implicit solvent model for CHCl$_3$.[47] Geometry reoptimizations were carried out first at the semiempirical AM1 level and then at the CAM-B3LYP/TZVP level with the PCM solvent model for both MeCN and acetone. Specific rotation data and single-point calculations for the sTDA ECD calculations were run with various functionals (B3LYP, BH&HLYP, CAM-B3LYP, and PBE0 for the SR and CAM-B3LYP, LC-BLYP, and ωB97X for the sTDA calculations) and the TZVP basis set as implemented in the Gaussian 09 package.[48] The sTDA calculations were performed with the sTDA 1.6 package.[49] Electronic circular dichroism spectra were generated as sums of Gaussians with 3000 cm^{-1} width at half-height, using dipole-velocity-computed rotational strength values.[50] Boltzmann distributions were estimated from the CAM-B3LYP/TZVP energies. The MOLEKEL software package was used for visualization of the results.[51]

ASSOCIATED CONTENT

Ⓢ Supporting Information

The Supporting Information is available free of charge at https://pubs.acs.org/doi/10.1021/acs.jnatprod.9b00655.

Low-energy conformers of (aS,12R,12$'R$)-**2**, 1D and 2D NMR and HRESIMS spectra of compounds **1**−**5**, and table of NMR data of diosmetin 7-O-[2,4-di-O-(α-L-rhamnopyranosyl)]-β-D-glucopyranoside; tables of Boltzmann populations and specific optical rotations of the low-energy conformers of (aS,12R,12$'R$)-**2** and (aR,12R,12$'R$)-**3** computed at various levels for the CAM-B3LYP/TZVP PCM/acetone reoptimized AM1 conformers (PDF)

AUTHOR INFORMATION

Corresponding Authors
*E-mail: kurtan.tibor@science.unideb.hu.
*E-mail: hohmann@pharm.u-szeged.hu.

ORCID Ⓘ
Tibor Kurtán: 0000-0002-8831-8499
Attila Mándi: 0000-0002-7867-7084
Judit Hohmann: 0000-0002-2887-6392

Notes
The authors declare no competing financial interest.

ACKNOWLEDGMENTS

REFERENCES

(1) Asakawa, Y.; Ludwiczuk, A.; Nagashima, F. *Phytochemistry* **2013**, *91*, 52−80.
(2) Asakawa, Y.; Ludwiczuk, A. *J. Nat. Prod.* **2018**, *81*, 641−660.
(3) Asakawa, Y. *Prog. Chem. Org. Nat. Prod.* **1982**, *42*, 1−285.
(4) Asakawa, Y. *Prog. Chem. Org. Nat. Prod.* **1995**, *65*, 1−618.
(5) Asakawa, Y.; Ludwiczuk, A.; Nagashima, F. *Prog. Chem. Org. Nat. Prod.* **2013**, *95*, 1−795.
(6) Glime, J. M. Medical Uses: Medical Conditions. Chapters 2−1. In *Bryophyte Ecology*, Vol 5; Glime, J. M., Ed.; Michigan Technological University and the International Association of Bryologists, 2017; pp 1−26.
(7) *Flora of North America*, Vol. 27, pp 395, 426, 427, 428. [Online] Available: http://www.efloras.org/florataxon.aspx?flora_id=1&taxon_id=200001018.
(8) Gellerman, J. L.; Anderson, W. H.; Schlenk, H. *Lipids* **1975**, *10*, 656−661.
(9) (a) Grimme, S. *J. Chem. Phys.* **2013**, *138*, 244104. (b) Risthaus, T.; Hansen, A.; Grimme, S. *Phys. Chem. Chem. Phys.* **2014**, *16*, 14408−14419. (c) Bannwarth, S.; Grimme, C. *Comput. Theor. Chem.* **2014**, *1040−1041*, 45−53. (d) Bannwarth, C.; Grimme, S. *J. Phys. Chem. A* **2015**, *119*, 3653−3662.
(10) (a) Bara, R.; Zerfass, I.; Aly, A. H.; Goldbach−Gecke, H.; Raghavan, V.; Sass, P.; Mándi, A.; Wray, V.; Polavarapu, P. L.; Pretsch, A.; Lin, W.; Kurtán, T.; Debbab, A.; Broetz-Oesterhelt, H.; Proksch, P. *J. Med. Chem.* **2013**, *56*, 3257−3272. (b) Rönsberg, D.; Debbab, A.; Mándi, A.; Vasylyeva, V.; Böhler, P.; Stork, B.; Engelke, L.; Hamacher, A.; Sawadogo, R.; Diederich, M.; Wray, V.; Lin, W.; Kassack, M. U.; Janiak, C.; Scheu, S.; Wesselborg, S.; Kurtán, T.; Aly, A. H.; Proksch, P. *J. Org. Chem.* **2013**, *78*, 12409−12425.
(11) (a) Li, X. L.; Kurtán, T.; Hu, J. C.; Mándi, A.; Li, J.; Li, X. W.; Guo, Y. W. *J. Agric. Food Chem.* **2017**, *65*, 1550−1555. (b) Wu, Q.; Yu, G.; Kurtán, T.; Mándi, A.; Peng, J.; Mo, X.; Liu, M.; Li, H.; Sun, X.; Li, J.; Zhu, T.; Gu, Q.; Li, D. *J. Nat. Prod.* **2015**, *78*, 2691−2698.
(12) Zhang, Q.; Mándi, A.; Li, S.; Chen, Y.; Zhang, W.; Tian, X.; Zhang, H.; Li, H.; Zhang, W.; Zhang, S.; Ju, J.; Kurtán, T.; Zhang, C. *Eur. J. Org. Chem.* **2012**, *2012*, 5256−5262.
(13) Polavarapu, P. L.; Jeirath, N.; Kurtán, T.; Pescitelli, G.; Krohn, K. *Chirality* **2009**, *21*, E202−E207.
(14) Li, J.; Seupel, R.; Bruhn, T.; Feineis, D.; Kaiser, M.; Brun, R.; Mudogo, V.; Awale, S.; Bringmann, G. *J. Nat. Prod.* **2017**, *80*, 2807−2817.
(15) Bringmann, G.; Mortimer, A. J. P.; Keller, P. A.; Gresser, M. J.; Garner, J.; Breuning, M. *Angew. Chem., Int. Ed.* **2005**, *44*, 5384−5427.
(16) Covington, C. L.; Junior, F. M. S.; Silva, J. H. S.; Kuster, R. M.; de Amorim, M. B.; Polavarapu, P. L. *J. Nat. Prod.* **2016**, *79*, 2530−2537.
(17) Frank, M.; Hartmann, R.; Plenker, M.; Mándi, A.; Kurtán, T.; özkaya, F. C.; Müller, W. E. G.; Kassack, M. U.; Hamacher, A.; Lin, W.; Liu, Z.; Proksch, P. *J. Nat. Prod.* **2019**, *82*, 2159−2166.
(18) Kicsák, M.; Mándi, A.; Varga, S.; Herczeg, M.; Batta, Gy.; Bényei, A.; Borbás, A.; Herczegh, P. *Org. Biomol. Chem.* **2018**, *16*, 393−401.
(19) Yanai, T.; Tew, D. P.; Handy, N. C. *Chem. Phys. Lett.* **2004**, *393*, 51−57.
(20) Iikura, H.; Tsuneda, T.; Yanai, T.; Hirao, K. *J. Chem. Phys.* **2001**, *115*, 3540−44.
(21) Chai, J.-D.; Head-Gordon, M. *J. Chem. Phys.* **2008**, *128*, 084106.
(22) (a) Polavarapu, P. L. *Chirality* **2008**, *20*, 664−672. (b) Sun, P.; Yu, Q.; Li, J.; Riccio, R.; Lauro, G.; Bifulco, G.; Kurtán, T.; Mándi, A.; Tang, H.; Li, T.-J. *J. Nat. Prod.* **2016**, *79*, 2552−2558.

(23) (a) Polavarapu, P. L. *Chirality* **2006**, *18*, 348−356. (b) Mándi, A.; Kurtán, T. *Nat. Prod. Rep.* **2019**, *36*, 889−918.

(24) Giorgio, E.; Viglione, R. G.; Zanasi, R.; Rosini, C. *J. Am. Chem. Soc.* **2004**, *126*, 12968−12976.

(25) Sun, Y. Z.; Kurtán, T.; Mándi, A.; Tang, H.; Chou, Y.; Soong, K.; Su, L.; Sun, P.; Zhuang, C. L.; Zhang, W. *J. Nat. Prod.* **2017**, *80*, 2930−2940.

(26) Mazzeo, G.; Longhi, G.; Abbate, S.; Buonerba, F.; Ruzziconi, R. *Eur. J. Org. Chem.* **2014**, *2014*, 7353−7363.

(27) Asakawa, Y.; Tori, M.; Takikawa, K.; Krishnamurty, H. G.; Kar, S. K. *Phytochemistry* **1987**, *26*, 1811−1816.

(28) Adam, P.; Becker, H. *Phytochemistry* **1993**, *35*, 139−143.

(29) So, M. L.; Chan, W. H.; Xia, P. F.; Cui, Y. *Nat. Prod. Lett.* **2002**, *16*, 167−171.

(30) Asakawa, Y. Chemical Constituents of the Bryophytes. In *Progress in the Chemistry of Organic Natural Products*; Kinghorn, A. D.; Falk, H.; Gibbons, S.; Kobayashi, J.; Asakawa, Y.; Liu, J.-K., Eds.; Spinger: Vienna, 1995; Vol. *65*.

(31) Asakawa, Y. *Phytochemistry* **2004**, *65*, 623−669.

(32) Anton, H.; Kraut, L.; Mues, R.; Maria, I.; Morales, Z. *Phytochemistry* **1997**, *46*, 1069−1075.

(33) Nagashima, F.; Momosaki, S.; Watanabe, Y.; Toyota, M.; Huneck, S.; Asakawa, Y. *Phytochemistry* **1996**, *41*, 207−211.

(34) Flegel, M.; Adam, K. P.; Becker, H. *Phytochemistry* **1999**, *52*, 1633−1638.

(35) Martini, U.; Zapp, J.; Becker, H. *Phytochemistry* **1998**, *47*, 89−96.

(36) Toyota, M.; Yoshida, T.; Kan, Y.; Asakawa, Y. *Tetrahedron Lett.* **1996**, *37*, 4745−4748.

(37) Krivoshchekova, O. E.; Stepanenko, L. S.; Mishchenko, N. P.; Denisenko, V. A.; Maksimov, O. B. *Chem. Nat. Compd.* **1983**, *19*, 270−274.

(38) Johnson, B. C.; Cohen, P.; Polonsky, J.; Lederer, E. *Nature* **1963**, *199*, 285−286.

(39) Krone, B.; Hinrichs, A.; Zeeck, A. *J. Antibiot.* **1981**, *34*, 1538−1543.

(40) Gould, S. J.; Melville, C. R.; Chen, J. *Tetrahedron* **1997**, *53*, 4561−4568.

(41) Majumder, P. L.; Sen, R. C. *Phytochemistry* **1991**, *30*, 2092−2094.

(42) Zhang, C.; Li, L.; Xiao, Y. Q.; Li, W.; Yin, X. J.; Tian, G. F.; Chen, D. D.; Wang, Y. *Chin. Chem. Lett.* **2010**, *21*, 816−817.

(43) Zylber, J.; Zissmann, E.; Polonsky, J.; Lederer, E.; Merrien, M. A. *Eur. J. Biochem.* **1969**, *10*, 278−283.

(44) Sargent, M. V.; Smith, D. N. *J. Chem. Soc. C* **1970**, 329−331.

(45) Tóth, B.; Hohmann, J.; Vasas, A. *J. Nat. Prod.* **2018**, *81*, 661−678.

(46) Österdahl, B. G. *Acta Chem. Scand.* **1978**, *32*, 714−716.

(47) *MacroModel*; Schrödinger, LLC, 2015, http://www.schrodinger.com/MacroModel.

(48) Frisch, M. J.; Trucks, G. W.; Schlegel, H. B.; Scuseria, G. E.; Robb, M. A.; Cheeseman, J. R.; Scalmani, V.; Barone, G.; Mennucci, B.; Petersson, G. A.; Nakatsuji, H.; Caricato, M.; Li, X.; Hratchian, H. P.; Izmaylov, A. F.; Bloino, J.; Zheng, G.; Sonnenberg, J. L.; Hada, M.; Ehara, M.; Toyota, K.; Fukuda, R.; Hasegawa, J.; Ishida, M.; Nakajima, T.; Honda, Y.; Kitao, O.; Nakai, H.; Vreven, T.; Montgomery, J. A., Jr.; Peralta, J. E.; Ogliaro, F.; Bearpark, M.; Heyd, J. J.; Brothers, E.; Kudin, K. N.; Staroverov, V. N.; Kobayashi, R.; Normand, J.; Raghavachari, K.; Rendell, A.; Burant, J. C.; Iyengar, S. S.; Tomasi, J.; Cossi, M.; Rega, N.; Millam, J. M.; Klene, M.; Knox, J. E.; Cross, J. B.; Bakken, V.; Adamo, C.; Jaramillo, J.; Gomperts, R.; Stratmann, R. E.; Yazyev, O.; Austin, A. J.; Cammi, R.; Pomelli, C.; Ochterski, J. W.; Martin, R. L.; Morokuma, K.; Zakrzewski, V. G.; Voth, G. A.; Salvador, P.; Dannenberg, J. J.; Dapprich, S.; Daniels, A. D.; Farkas, Ö.; Foresman, J. B.; Ortiz, J. V.; Cioslowski, J.; Fox, D. J. *Gaussian 09* (Revision E.01); Gaussian, Inc.: Wallingford, CT, 2013.

(49) Grimme, S.; Bannwarth, C.; Shushkov, P.; de Wergifosse, M. *sTDA - A Program Package to Calculate Excited States via a Simplified Tamm-Dancoff Approximation to TD-DFT Version 1.6*; Mulliken Center for Theoretical Chemistry Institut für Physikalische und Theoretische Chemie der Universität Bonn: Bonn, Germany, 2018.

(50) Stephens, P. J.; Harada, N. *Chirality* **2009**, *22*, 229−233.

(51) Varetto, U. *MOLEKEL 5.4*; Swiss National Supercomputing Centre: Manno, Switzerland, 2009.